Nanoindentation as a Probe for Mechanically-Induced Molecular Migration in Layered Organic Donor–Acceptor Complexes

ARTICLE *in* CHEMISTRY - AN ASIAN JOURNAL · SEPTEMBER 2012

Impact Factor: 4.59 · DOI: 10.1002/asia.201200224 · Source: PubMed

CHEMISTRY
AN ASIAN JOURNAL

DOI: 10.1002/asia.201200224

Nanoindentation as a Probe for Mechanically-Induced Molecular Migration in Layered Organic Donor–Acceptor Complexes

Sunil Varughese,[a] Mangalampalli S. R. N. Kiran,[b] Upadrasta Ramamurty,*[b] and Gautam R. Desiraju*[a]

Abstract: Nanoindentation and scratch experiments on 1:1 donor–acceptor complexes, **1** and **2**, of 1,2,4,5-tetracyanobenzene with pyrene and phenanthrene, respectively, reveal long-range molecular layer gliding and large interaction anisotropy. Due to the layered arrangements in these crystals, these experiments that apply stress in particular directions result in the breaking of interlayer interactions, thus allowing molecular sheets to glide over one another with ease. Complex **1** has a layered crystal packing wherein the layers are 68° skew under the (002) face and the interlayer space is stabilized by van der Waals interactions. Upon indenting this surface with a Berkovich tip, pile-up of material was observed on just one side of the indenter due to the close angular alignment of the layers with the half angle of the indenter tip (65.35°). The interfacial differences in the elastic modulus (21%) and hardness (16%) demonstrate the anisotropic nature of crystal packing. In **2**, the molecular stacks are arranged in a staggered manner; there is no layer arrangement, and the interlayer stabilization involves C–H···N hydrogen bonds and π···π interactions. This results in a higher modulus (20%) for (020) as compared to (001), although the anisotropy in hardness is minimal (4%). The anisotropy within a face was analyzed using AFM image scans and the coefficient of friction of four orthogonal nanoscratches on the cleavage planes of **1** and **2**. A higher friction coefficient was obtained for **2** as compared to **1** even in the cleavage direction due to the presence of hydrogen bonds in the interlayer region making the tip movement more hindered.

Keywords: charge-transfer complexes · layered compounds · mechanical anisotropy · molecular migration · nanoindentation

Introduction

Molecular migration within crystalline solids is of topical concern and it underlies phenomena such as solid-state reactivity, cocrystal formation, and defect transport.[1] Although classical topochemistry envisages minimum atomic or molecular mobility in crystalline solids,[2] Kaupp has suggested that long-range molecular migrations are the reason for the nearly 100% yields achieved in many solid-state reactions that are supposedly (or nominally) governed by topochemistry.[3] Solid-state chemical reactions and the consequent changes in molecular geometry induce molecular movements that release the internal pressure created during the initial reaction.[4] These molecular transits extend from small-range molecular rearrangements to long-range diffusion, as seen in the formation of molecular complexes, such as the one formed between picric acid and naphthalene.[5] Such migrations can also be artificially induced by applying mechanical stress using indentation or nanoscratching.[6] While techniques such as X-ray diffraction and spectroscopy generally fail to perceive the resulting anisotropic migrations, atomic force microscopy (AFM)[7] and grazing incidence diffraction (GID)[8] can detect such effects unambiguously. Nanoindentation is an effective technique for the precise mechanical characterization of small-volume materials such as thin films and single crystals.[9] Whereas its utility in the characterization of inorganic and engineering materials is ubiquitous, only a limited number of studies have been reported for molecular crystals.[10,11] These include our recent report on the mechanical anisotropy in saccharin[12] and a study on interaction anisotropy and shear instability of aspirin polymorphs.[13]

In layered structures, strong interactions constitute the layers while weak interactions in the interlayer region bind the layers together in a stack so that the packing is distinctly anisotropic. Such materials range from structures with atomic thickness, like in graphite, to macrostructures such as lamellar clays. Layered compounds are of interest due to their utility as intercalates, lubricants, and conducting materials.[14] Mechanical shearing and bending of their crystals is an important consequence of the packing anisotropy and

[a] Dr. S. Varughese, Prof. G. R. Desiraju
Solid State and Structural Chemistry Unit
Indian Institute of Science
Bangalore 560 012 (India)
Fax: (+91) 080-23602306
E-mail: desiraju@sscu.iisc.ernet.in

[b] Dr. M. S. R. N. Kiran, Prof. U. Ramamurty
Department of Materials Engineering
Indian Institute of Science
Bangalore 560 012 (India)
E-mail: ramu@materials.iisc.ernet.in

Supporting information for this article is available on the WWW under http://dx.doi.org/10.1002/asia.201200224.

the nonspecific nature of interactions in the interlayer region.[15] These anisotropic effects can also lead to polymorphic forms with diverse mechanical properties, enabling their mechanical sorting.[16] Pyrazine-2-carboxamide, venlafaxine hydrochloride, and 6-chloro-2,4-dinitroaniline are layered compounds with distinct mechanical properties among the polymorphs.[17] Further to mechanical evaluation, the directional nature of thermal expansion and high-pressure studies can also provide information regarding the anisotropy in molecular crystals.[18]

Charge-transfer complexes (CT complexes) or electron donor–acceptor complexes often have layered structures in which planar aromatic donors and acceptors are involved. Molecules are stabilized through electrostatic attractions wherein fractional charge is transferred between the molecular entities.[19] This attraction, generally created by an electronic transition to an excited electronic state, is much weaker than covalent bonding. Since the excitation energy of this resonance occurs frequently in the visible region of the electromagnetic spectrum, it usually imparts an intense color to the complexes. 1,2,4,5-Tetracyanobenzene (TCNB) is well known for its ability to make CT complexes with aromatic donors. In this study, 1:1 complexes of TCNB with pyrene (**1**) and phenanthrene (**2**) were used to evaluate the mechanical properties of anisotropic layered solids. Indentation experiments were carried out using a sharp-tipped Berkovich indenter to characterize a range of mechanical properties including elastic modulus, hardness, fracture behavior, and molecular migration under mechanical stress.

Abstract in Sanskrit:

स्फटिकेषु विद्यमानानां नानाविध-अण्विकचेष्टितानां पारिमाणिकरीत्या प्रायोगिकतोलनाय परमसूक्ष्म-भङ्गुरीकरणं सदवकाशदायकं चकास्ति। पैरीन् तथा च फिनान्त्रीन्-अणुसहित 1,2,4,5-टेट्रा-सयनो-बेन्जीन् इत्यस्य दातृ-स्वीकर्तृसङ्कीर्णयोः (इतः परं 1 तथा च 2, क्रमेण) परमसूक्ष्म-भङ्गुरीकरण-कण्डूयन-प्रयोगौ क्रमेण परस्परचेष्टितलक्षणेषु महतीं विषमदिशात्मकतां, दीर्घश्रेणीय-विषमदिशात्मक-अणुस्तर-निस्यन्दनं च प्रकटीकुरुतः। सङ्कीर्णस्तरविन्यासमनुसृत्य भङ्गुरीकरण-कण्डूयन-प्रयोगौ अन्तस्स्तरीयचेष्टितावघातिनौ भूत्वा अणुस्तरान्योन्यनिस्यन्दनाय आनुकूल्यं जनयतः। स्तरीभूतस्फाटिकसञ्चये प्रथमसङ्कीर्णे (1) अणुस्तराः {002} मुखस्य अधस्तात् 68° अनृजुदिशि विन्यस्ताः, वेण्डर् वाल् बलैः स्थिरीकृत-अन्तस्स्तरीयान्तराश्च वर्तन्ते। मुखस्यास्य बेर्कोविच् वाज्रिकसूचीं उपयुज्य भङ्गुरीकरणानन्तरं सूच्याः एकस्मिन्नेव पार्श्वे विरूपितपदार्थस्य राशीभवनं दर्शितम्, यतः अणुस्तराणां कोणीयविन्यासः सूच्याः अर्धकोणदिशं (65.35°) अनुगम्यते। स्थितिस्थापकगुणकभिन्नता (21%), काठिन्यभेदः (16%) च विषमदिशात्मकस्फाटिकविन्यासं प्रमाणयतः। द्वितीयसङ्कीर्णे (2) अणुस्तराः विचलिताः, समुचितस्तरविन्यासरहिताः च। सङ्कीर्णेऽस्मिन् C–H···N उदजनीयबन्धाः, π···π बन्धाश्च अन्तस्स्तरीयान्तर-स्थिरीकरणहेतवः भवन्ति। अतः {020} मुखस्य स्थितिस्थापकगुणकवृद्धिः (20%, {001} अपेक्षया) सम्पन्नः, यद्यपि काठिन्यभेदः न्यून एव (4%)। स्फटिकस्तरविदलनदिशायामपि अन्तस्स्तरीय-उदजनिबन्धैः सूचीगमनदिशानिर्देशनात् द्वितीयसङ्कीर्णस्य घर्षणगुणकं प्रथमसङ्कीर्णस्य घर्षणगुणकात् अधिकं अजायत।

Results and Discussion

Pyrene Complex

The 1:1 TCNB-pyrene complex (**1**) crystallizes in the monoclinic system and the molecules make a layered arrangement;[20] (100) and (002) constitute the significant faces with (002) being the major one (Figure 1). While the mean plane of the molecular layers makes an angle of 25° with (100),

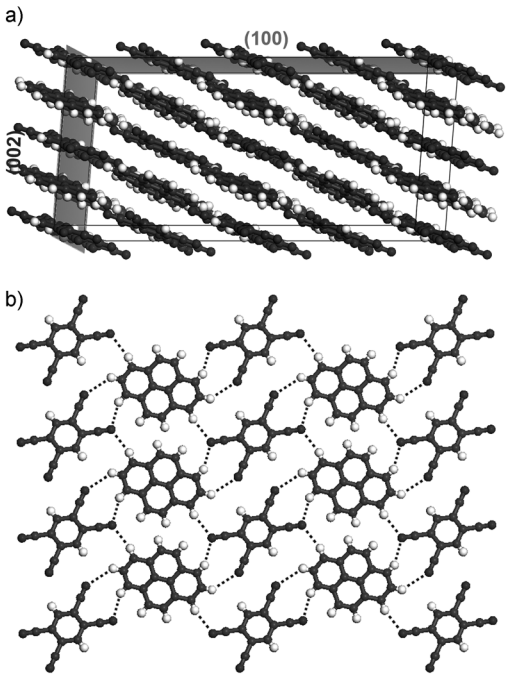

Figure 1. Crystal packing of **1**. a) Layer arrangement. b) Interactions in an individual layer.

they are 68° skew under (002). The interplanar spacings, d, are 7.138 and 7.747 Å for the (100) and (002) orientations, respectively. Within an individual layer, TCNB and pyrene interact through several C–H···N hydrogen bonds with an average H···N distance of 2.72 Å. The average interlayer (π···π) separation is 3.45 Å. Significant interaction anisotropy manifests itself as differences in the attachment energies, E_{att}, for the (100) and (002) faces as −33.699 and −23.947 kJ mol^{-1}, respectively.

Both the load–penetration depth curves (P–h curves) and the H and E values obtained for the (100) and (002) faces of **1** indicate significant mechanical anisotropy in the crystals examined. The P–h curves show large residual depths upon unloading, which indicates that the crystal undergoes significant plastic deformation upon indentation (Figure 2). Interestingly, both curves show similar penetration depths; however, the loading part of the curves is distinct in nature: while the loading part of the P–h curve obtained on the (002) face is smooth, several distinct displacement bursts are observed on (100). The average values of H and E are 0.120 ± 0.001 and 3.92 ± 0.054 GPa for (002), and 0.143 ±

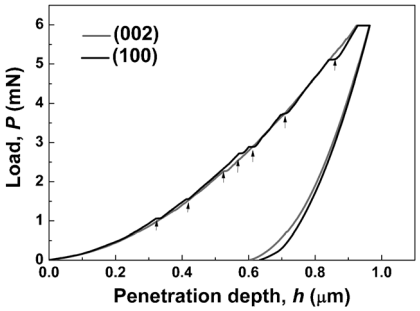

Figure 2. Representative *P–h* curves obtained on two faces of a crystal of **1**.

0.01 and 4.98 ± 0.249 GPa for (100), respectively. The error bars correspond to the standard deviations obtained for 15 measurements made on each crystal face. The large difference (21%) in the moduli for the crystal faces suggests significant dissimilarities in the interaction characteristics. Further, the large degree of anisotropy in H (16%) suggests possible differences in the micromechanisms of plasticity. On the *P–h* curve of (100) of **1**, the first significant displacement burst (pop-in) was consistently observed to occur at 1.05 ± 0.1 mN with a magnitude, h_{pop-in}, of about 21 nm. Increasing the load results in several pop-ins with h_{pop-in} of 7 and 13 nm, with the largest one being 21 nm. It is clear that h_{pop-in} is in multiples of 7 nm which in turn is an integral multiple of $d_{(100)}$ (7.138 Å). In an earlier study on crystalline saccharin, we have also noted such a correspondence between the pop-in magnitude and the underlying crystal length scale.[12]

The AFM images of the indents on (002) show a significant pile-up of material along one of the faces of the indenter (Figure 3a), whereas no pile-up is observed in the case of indentation on the (100) face (Figure 3b). The quantity and shape of the profiles of the pile-up strongly depends on the layer orientation and the tip geometry. The indenter tip used in the present study has a total included angle of 142.3° with a half angle of 65.35°. The molecular layers at an angle of 68° with the (002) face and the indenter half angle are aligned closely (Figure 3c and 3d), thereby enabling the layers to slide over the edge of the indenter tip. This is analogous to the sliding of the tectonic plates during convergent continental collision.[21] However, due to the slant arrangement of the layers, they get compressed in the other orientations, thus resulting in pile-up in one orientation only.

The discrete displacement bursts in the *P–h* curve obtained on (100) can be correlated with the crystallographic features. As discussed by us earlier, plastic deformation in layered organic crystals can be attributed to slipping along a crystallographic plane when sheets of molecules glide across one another, similar to a stack of playing cards in a deck.[16b] Generally, the primary slip plane in organic materials is assumed to be the weakest bound plane in that the attachment energy for this plane is the least. Accordingly, slipping is preferred along this plane. By this token, the pop-ins observed in the (100) orientation are surprising because it corresponds to the plane with the largest attachment energy. However, the presence of molecular layers with weakly bound interlayer spaces normal to the indentation direction makes such a slip possible. In these cases the slip occurs for the planes that are the most widely spaced with the smallest E_{att} and in the directions that are closest packed so that the slip vector is the smallest. Hence, the possible slip system in **1** could be $\{100\}<002>$. The absence of any directional interactions along $<002>$ makes gliding of the planes without much shear resistance viable. This observation agrees with the proposal by Olusanmi et al.[22] that, for aspirin, low attachment energy alone is not a sufficiently reliable indication of a cleavage plane. The absence of material pile-up in the case of indentation on the (100) face can be due to the effective compressible deformation nature of the π···π interactions as the indentation is performed along the interaction directions.

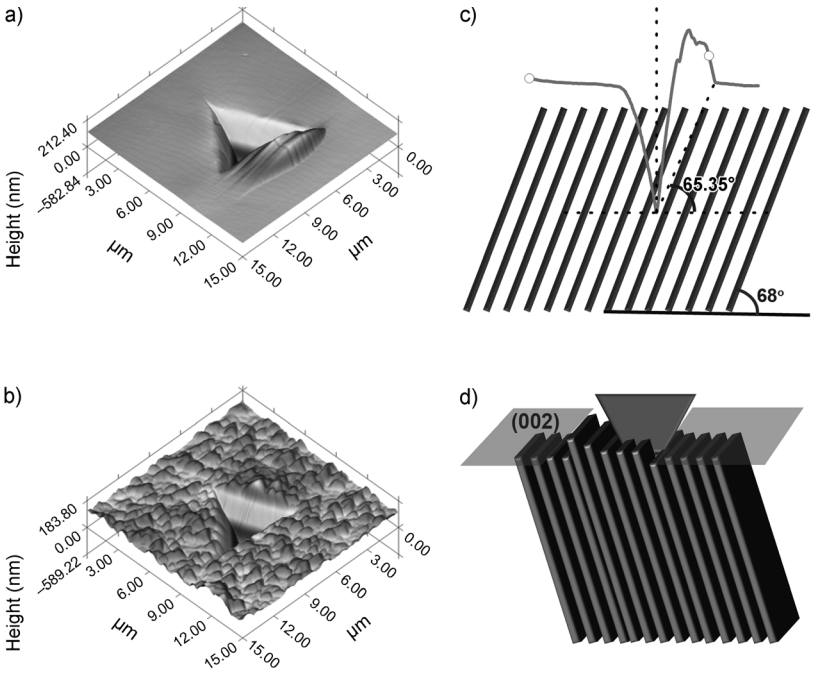

Figure 3. 3D representation of AFM images of the residual indent impressions on a) (002) and b) (100) of crystals of **1**. c) Representation of the angular alignment of the layers with the half angle of the Berkovich tip. The grey curve is the line profile drawn at the middle of the residual indent impression of (002). d) Schematic representation of the layer sliding along the side of the indenter tip.

These observations provide a possible explanation for pop-ins only on the (100) face. On indenting along [100], the layers are compressed due to the presence of weak van der Waals interactions until they come close enough to activate a repulsion. This permits the broken/stretched layers to rearrange themselves so that some of the stored elastic strain energy is released, which in turn results in the gliding of the layers, the energetically most viable option available to the system. All this affects the sudden penetration of the indenter tip into the sample and is observed as pop-ins on the *P–h* curve. These pop-ins therefore reveal a release of internal pressure. However, along [002], the tip penetrates the crystal perpendicular to the stacking direction, thus enabling the molecular layers, which are stabilized through weak non-directional π···π interactions, to slide past one another with ease; this appears as a smooth *P–h* curve. To put these results in perspective, it may be stated that the absence of pop-ins in the *P–h* curve corresponding to (002) is due to the availability of more slip planes.

Phenanthrene Complex

Unlike the pyrene complex, the TCNB complex with phenanthrene (**2**) is composed of trimer units (one TCNB and two phenanthrene molecules) stacked in a staggered manner.[23] Crystals of **2** are mainly constituted of two sets of faces: (001) and (020), of which the latter is the major face. The molecules stack down $<001>$ and adjacent stacks are linked with C–H···N interactions (Figure 4). While molecular stacks make an angle of 21° with (001), they are perpendicular to the (020) face. However, due to the staggered arrangement of the molecules, the formation of a layered structure is not observed. The C–H···N hydrogen bonds are inclined to the layer and contribute along with the π···π interactions to the stabilization of the stacking arrangement of the molecules. The *d*-spacing for (001) and (020) orientations is 7.157 and 6.517 Å, respectively, with corresponding attachment energies of −34.828 and −23.705 kJ mol^{-1}.

The observed dissimilarity in the crystal packing in **2**, with respect to **1**, is reflected in the mechanical behavior as well. The maximum penetration depth at a peak load of 6 mN for **2** is less than in **1** (Figure 5). The *P–h* curve obtained on (020) exhibits some serrations while pop-ins are observed on (001). The crystal undergoes substantial plastic deformation as evident from the large residual depth upon unloading. The average *H* and *E* values obtained on (020) are 0.140 ± 0.001 and 5.76 ± 0.115 GPa, while that for (001) are 0.146 ± 0.001 and 4.59 ± 0.081 GPa, respectively. Thus, (020) is stiffer by 20% while (001) is harder by 4%. Hence, a significant anisotropy in *E* exists although *H* is comparable. The latter can be due to the effect of the staggered arrangement of the layers and the slanted orientation of C–H···N hydrogen bonds, thus allowing the interactions to make contributions in both faces. The first significant displacement burst in the *P--h* curve obtained on (001) is 13 nm in magnitude and the load at which it occurs is consistent at 0.7 ± 0.05 mN. In addition, a few small pop-ins with a magnitude of 7 nm are seen on the loading part of the *P–h* curve and it should be noted that the pop-in magnitude is again an integral multiple of $d_{(001)}$ (7.157 Å).

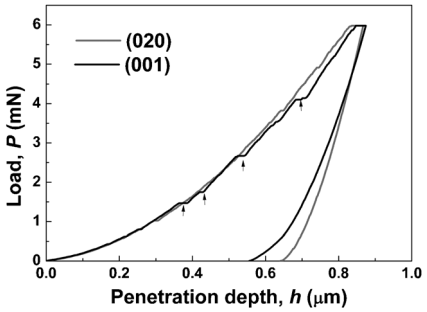

Figure 5. Representative *P–h* curves obtained on (020) and (001) of crystals of **2**.

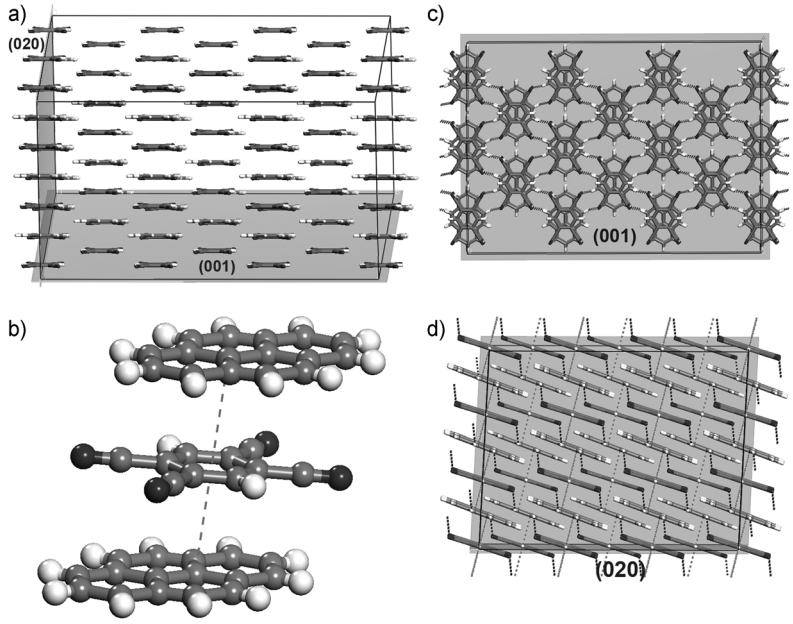

Figure 4. Crystal structure of **2**. a) Molecular arrangement with respect to the (020) and (001) plane. b) The trimer arrangement of the complex. c) The molecular arrangement down [001]. d) The molecular arrangement down [020].

The AFM images of the indent impressions on (020) show possible slip steps on the surface of the crystal (Fig-

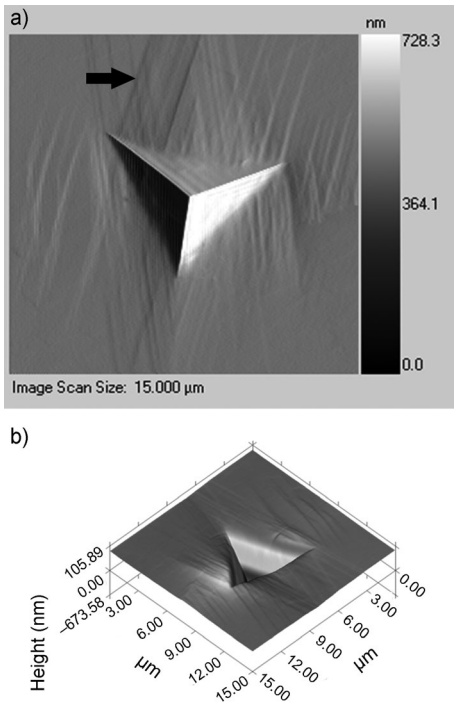

Figure 6. AFM image of the residual indent obtained on a) (020) of a crystal of **2**. b) 3D representation. The arrow shows the presence of slip lines in various directions.

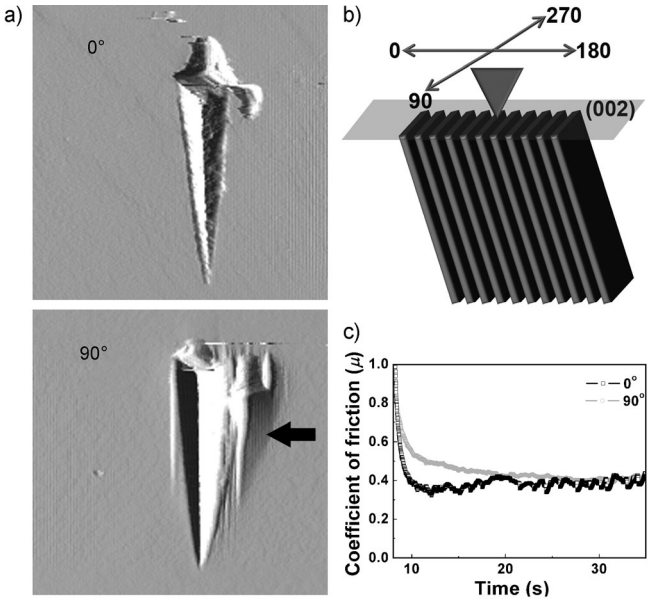

Figure 7. a) AFM images of a nanoscratch on (002) of crystals of **2**. b) Schematic representation of the tip movement during the nanoscratch experiments. c) The coefficient of friction at 0° and 90°.

ure 6a), possibly due to the broken layer arrangement of the molecular units and its deformation under the compressive stress brought about by the pyramidal geometry of the indenter tip. This deformation of layers is analogous to the distortion generated upon inserting a pencil point between the pages of a book. Furthermore, it is evident from the scan images that the indentation results in 'sinking in' of the material (Figure 6b). By contrast, indenting on (100) results in fracture; this is not surprising due to its greater hardness.

Nanoscratch Experiments

Nanoscratching is an effective probe for the molecular packing in various faces in different orientations and can further provide insights into mechanically induced molecular migrations that occur without chemical transformations.

In **1** the layered structure is such that intra- and interlayer interactions are quite distinct. This anisotropy means that the crystal can be cleaved easily along the layers. The layers are 68° skew under (002). Such an arrangement can yield distinct molecular migration events upon scratching at various orientations. In our experiments, four orthogonal directions yielded distinct scratch profiles and coefficient of friction, μ (ratio of lateral force to normal force) values, and the results may be correlated with the crystal packing. Scratching along the long crystal edge (0°) results in molecular migration on both sides together with a small pile-up of material at the end of the scratch. At 90°, molecules migrate only to the right hand side; AFM images show layer migration that is more evident towards the right hand side (Figure 7a). A significant molecular pile-up was noted on both the front and on either side of the scratch when the tip traverses at 0° and 180°. At 270° the molecules migrate only to the left hand side (scratch images of 180° and 270° are shown in Figure S1 in the Supporting Information). At 0° the tip moves along the skew direction of the layers and thus the layers are open for the release of material on either side of the scratch; at 180° the tip traverses against the skew direction and thus experiences the maximum friction, and moreover makes the largest material pile-up on both sides of the scratch as well as in the front (Figure 7b). This postulation is further substantiated by comparing the coefficient of friction values; 0° and 180° experience the lowest (μ_{avg} = 0.4) and highest friction (μ_{avg} = 0.5), respectively (Figure 7c).

In the 90° and 270° settings, the tip movement is relatively featureless, even without much variation in the coefficient of friction, and such a movement is due to the weak nature of the interlayer interactions making the slip rather smooth. Such anisotropy can be observed in organic molecular crystals with cleavage planes; good examples of molecular migration that takes place under mechanical stress are provided by thiohydantoin and anthracene.[3a] Because of the flat orientation of the molecular layers with respect to (100), scratch experiments on this face yielded only abrasions with small material pile-up at the end of the scratch, irrespective of the scratch direction. Such behavior is due to the restricted molecular migration within molecular layers upon scratching, and the pile-up could be due to the shifting of some fragments of the anisotropic monolayers in front of the tip. The migration distance (the distance affected from the middle of the scratch to the side) due to the indenter movement at 90° and 270° is 3.8 µm and the distance be-

tween slip lines is estimated as 700 nm, which is an integral multiple of $d_{(100)}$ as shown in Figure S2 in the Supporting Information.

For **2** in which the layers are oriented perpendicular to (020), a different scenario exists. The discontinuous layers with a staggered arrangement could result in interlocking which in turn would lead to reduced indenter movement. On (020) at 0°, when the tip traverses along the cleavage plane, no material pile-up was noticed although AFM images provide evidence of a limited layer movement (Figure 8a). At 90°, the movement is across the cleavage plane and the tip experiences uneven friction (evident from the jagged profile) brought about by the vertical layer arrangement (Figure 8b). This results in material pile-up at the end of the scratch. The tip again makes a smooth movement upon scratching the surface at 180° since it moves along the cleavage plane. Similar to the scratch at 90°, the tip movement at 270° resulted only in abrasion with a small pile-up (AFM scratch images for 180° and 270° are shown in Figure S3 in the Supporting Information). The friction coefficient for 90° and 270° indicates the presence of several uneven events that are due to the tip movement across the cleavage plane. The distances between the two consecutive troughs, where the friction coefficient falls sharply, are 210, 260, and 340 nm, respectively, and are closely related to the multiples of $d_{(020)}$ (6.517 Å).

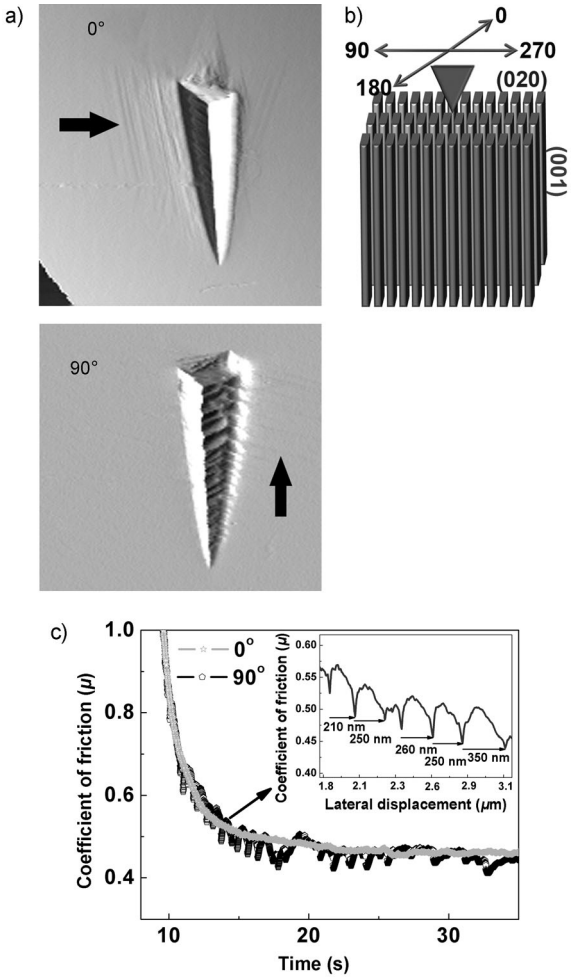

Figure 8. a) AFM images of the nanoscratch on (020). b) The coefficient of friction at 0° and 90° (the inset shows the analysis of the distance between the two consecutive troughs where the friction coefficient sharply decreases). c) Schematic representation of the tip movement during the nanoscratch experiments.

In both 0° and 90° scratch orientations, the tip experiences uniform friction and this is due to smooth sliding through the cleavage plane. However, the friction coefficient obtained from 0° and 90° in crystals of **2** is higher than the values obtained for **1** (90 and 270°), although the tip movements in both cases are along the cleavage plane. This higher magnitude could be the collective outcome of the presence of interlayer hydrogen bonds together with the broken layers in **2,** which hinder free movement of the indenter. On (001), scratching along orthogonal directions yielded only abrasions due to the flat orientation of the molecular layers, and the pyramidal tips efficiently obstruct upward migration of flat layers (Figure S4 in the Supporting Information). The migration distance by indenter movement on **2** at 0° and 180° is higher (i.e., 5 μm) and is brought about by the staggered arrangement of the discontinuous layers. The distance between slip lines is 350 nm, which is an integral multiple of $d_{(001)}$ (Figure S5 in the Supporting Information). While scratching at 90°, the indenter encounters a slip–slide mechanism (Figure S6 in the Supporting Information). The line profile on the slip–slide portion revealed that the height of the pile-up increases with increasing scratch load together with a periodic increment and decrement in the friction coefficient. As the indenter passes in a direction perpendicular to the layer arrangement, a few layers collectively create a resistance against indenter movement; however, with increasing lateral force they break up to release their stored elastic strain energy, thus resulting in a sudden fall in the friction coefficient. Since this process is continuous, a wavy movement of the indenter is observed.

Structure–Property Correlations

Due to the layered crystal structures, **1** and **2** exhibit large anisotropies in their mechanical properties, which can be correlated well with their crystal structures. Although the maximum penetration depths observed for both compounds are similar, the slope of the unloading segment is unique to each crystal facet, which indicates significant elastic anisotropy. This markedly dissimilar modulus values signify a strong correlation between stiffness and the underlying crystalline structure. The maximum change in modulus in **1** is 21% with (100) being the stiffest, while for **2** (020) is stiffer by 20%. This high degree of elastic anisotropy, as compared to that in our earlier reports, is due to the layered molecular arrangement. However, the magnitude of anisotropy is modest as compared to that seen in organic–inorganic hybrid layered compounds wherein the anisotropy is of the order of 77%.[24] This distinction is due to the fact that hydrogen bonds such as C–H···N (5 kJ mol^{-1}), within

the layers of **1** and **2**, are much weaker than most of the coordination bonds (50–200 kJ mol^{-1}) in the hybrid compounds. The interlayer bonds consisting of van der Waals forces (< 5 kJ mol^{-1}) are relatively weak and hence there is a lower modulus in **1**. However, the absence of a continuous layer and the presence of C–H···N hydrogen bonds in addition to π···π interactions in the interlayer space make (020) of **2** stiffer.

Unlike E, H is a function of test methods and various other parameters such as indenter tip geometry, applied load, and penetration depth; hence, it cannot be considered as an intrinsic material property. The plastic deformation is understood in terms of nucleation, rapid multiplication, and propagation of dislocations in metals and semiconductors, while in amorphous materials it arises due to shear bands. However, in molecular crystals, molecular sheets glide past one another along specific crystallographic planes resulting in plastic deformation. For **1**, the anisotropy in H is 16% and for **2** it is only 4%. The continuous layer structure in **1** and the absence of directional interaction in the interlayer region make the slip more facile. In **2**, the layers in [020] are stabilized through both C–H···N and π···π interactions and this makes the slip comparatively demanding. In addition, the breaking of directional C–H···N hydrogen bonds, which are responsible for interlayer binding, appears as serrations on the P–h curves.

Conclusions

Large anisotropy in interaction characteristics and long-range molecular layer gliding in organic charge-transfer complexes of 1,2,4,5-tetracyanobenzene (TCNB) with pyrene (**1**) or phenanthrene (**2**) have been unambiguously established using nanoindentation and scratch experiments. The layered crystal packing in **1** with layers that are 68° skew under the (002) face yields material pile-up in just one orientation. This is due to the large structural anisotropy in the intra- and interlayer regions along with a close alignment in the angular orientation with the half angle of the Berkovich indenter tip. The interaction anisotropy and the layered nature of crystal packing are evident from the large anisotropy existing between (100) and (002) in the elastic modulus (21%) and hardness (16%). The discontinuous molecular stacks, arranged in a staggered manner, result in a higher modulus of (020) (20%) as compared to (001), since both C–H···N hydrogen bonds and π···π interactions are present in the interlayer region. This difference in crystal packing is further demonstrated by AFM image scans and by analyses of the friction coefficients of four orthogonal nanoscratches on the cleavage planes of **1** and **2**. Depending on the orientation of the tip movement with respect to the orientation of the cleavage plane, the indenter experiences distinct friction coefficient and layer migration. However, for crystals of **2**, the tip experiences a higher friction coefficient with respect to **1**, even in the cleavage direction, due to the presence of hydrogen bonds in the interlayer region, which make the indenter movement more demanding. Thus, further to the mere evaluation of the crystal anisotropy in terms of structure, nanoindentation can be used as a tool to study layered crystal packing and molecular migration in molecular crystals. This study adds a new dimension to the understanding of structure–property relationships such as softness of layered crystals and deformation mechanisms, thus quantifying mechanical anisotropy and molecular migration in terms of crystal packing. In conclusion, nanoindentation of molecular crystals is a promising technique with significant implications in various aspects of solid-state chemistry and crystal engineering.

Experimental Section

Complex Preparation

A 1:1 mixture of TCNB and pyrene or phenanthrene was ground in the presence of a few drops of methanol (solvent-drop grinding). The pyrene mixture turned deep red while the phenanthrene mixture became orange. The respective complexes were dissolved in various solvents and solvent mixtures. While an acetone–ethyl acetate mixture yielded blocks of the pyrene complex, small blocks of the phenanthrene complex were obtained from acetone. These crystals were of a quality suitable for nanoindentation; in other words, they were large enough and with well-developed faces.

Nanoindentation

The crystals were firmly mounted on a stud using cyanoacrylate glue such that two different crystallographic faces can be indented. Indentation experiments were performed on these facets using a Triboindenter (Hysitron, Minneapolis, USA) with in situ AFM imaging capability. The machine continuously monitors the load, P, and depth of penetration, h, of the tip with force and displacement resolutions of 1 nN and 0.2 nm, respectively. A Berkovich diamond indenter with a tip radius of 100 nm was used. Before the indentations, crystal surfaces were imaged in the AFM mode in order to find relatively smooth regions. A peak load, P_{max}, of 6 mN, with loading and unloading rates of 0.6 mN s^{-1} and a hold time (at P_{max}) of 30 s, was employed. Post-indentation images of the impressions were captured immediately to avoid any time-dependent elastic recovery. A minimum of fifteen indentations were performed in each case and the average of them is reported. The P–h curves were analyzed using the Oliver–Pharr method[25] to extract the elastic modulus, E, of the crystal. However, this method was not employed for estimating the hardness, H, as pile-up of material against the indenter faces (which is due to the plastic flow) can lead to an overestimation of H. Hence, H was determined as P_{max}/A, where A is the contact area estimated from AFM images of the indentation impressions. Nanoscratch experiments were performed with a ramping force (normal force increasing with time) of 3.33 N ms^{-1}. In all cases, 10 μm long scratches were made. The experimental methodology has been already reported.[26]

X-Ray Crystallography

Single-crystal X-ray diffraction data were collected at low temperature (150 K) on a Rigaku Mercury 375R/M CCD (XtaLAB Mini) diffractometer using graphite monochromated $Mo_{K\alpha}$ radiation, equipped with a Rigaku low-temperature gas spray cooler. The detailed description of the experiment is provided in the Supporting Information. CCDC 869505 (**1**) and CCDC 869504 (**2**) contain the supplementary crystallographic data for this paper. These data can be obtained free of charge from the Cambridge Crystallographic Data Centre via www.ccdc.cam.ac.uk/data_request/cif.

Attachment Energy Calculations

Potential slip planes for the complexes were determined from the attachment energy of various predicted crystallographic planes. The attachment energy (E_{att}) is defined as the energy released on attachment of a growth slice to a growing crystal face. Thus, $E_{att} = E_{latt} - E_{slice}$, where E_{latt} is the lattice energy of the crystal and E_{slice} is the energy that is released on the formation of a growth slice of a thickness equal to the *d*-spacing for the crystallographic plane that represents a face. The Dreiding 2.21 (Materials Studio 4.4) force field was used to calculate the attachment energies of various faces of the complexes. The complexes consist of layers of molecules stabilized through hydrogen bonds and stacking interactions.

Acknowledgements

S.V. thanks the Department of Science and Technology for a Young Scientist Fellowship. M.S.R.N.K thanks The University Grants Commission for a Dr. D. S. Kothari Post-Doctoral Fellowship. G.R.D thanks DST for a J. C. Bose Fellowship. The authors thank Mr. V. S. S. Pavan Kumar Hari (Electrical Engineering, IISc) for help in preparing the abstract in Sanskrit.

[1] a) K. Chadwick, R. Davey, W. Cross, *CrystEngComm* **2007**, *9*, 732–734; b) R. Kuroda, K. Higashiguchi, S. Hasebe, Y. Imai, *CrystEngComm* **2004**, *6*, 463–468; c) G. Kaupp, *Curr. Opin. Solid State Mater. Sci.* **2002**, *6*, 131–138; d) G. Kaupp, J. Schmeyers, *Angew. Chem.* **1993**, *105*, 1656–1658; *Angew. Chem. Int. Ed.* **1993**, *32*, 1587–1589; e) R. B. Godiksen, Z. T. Trautt, M. Upmanyu, J. Schiotz, D. J. Jensen, S. Schmidt, *Acta Mater.* **2007**, *55*, 6383–6391.

[2] a) G. M. J. Schmidt, *J. Chem. Soc.* **1964**, 2014–2021; b) G. M. J. Schmidt, *Pure Appl. Chem.* **1971**, *27*, 647–678.

[3] a) G. Kaupp, M. R. Naimi-Jamal, *CrystEngComm* **2005**, *7*, 402–410; b) G. Kaupp, *Top. Curr. Chem.* **2005**, *254*, 95–183.

[4] C. Karunatilaka, D. K. Bučar, L. R. Ditzler, T. FriŠčič, D. C. Swenson, L. R. MacGillivray, A. V. Tivanski, *Angew. Chem.* **2011**, *123*, 8801–8805; *Angew. Chem. Int. Ed.* **2011**, *50*, 8642–8646.

[5] R. P. Rastogi, N. B. Singh, *J. Phys. Chem.* **1968**, *72*, 4446–4449.

[6] G. Kaupp, J. Schmeyers, U. D. Hangen, *J. Phys. Org. Chem.* **2002**, *15*, 307–313.

[7] G. Kaupp, *CrystEngComm* **2003**, *5*, 117–133.

[8] A. Herrmann, G. Kaupp, T. Geue, U. Pietsch, *Mol. Cryst. Liq. Cryst.* **1997**, *293*, 261–275.

[9] A. Gouldstone, N. Chollacoop, M. Dao, J. Li, A. M. Mino, Y. L. Shen, *Acta Mater.* **2007**, *55*, 4015–4039.

[10] a) M. S. R. N. Kiran, S. Varughese, U. Ramamurty, G. R. Desiraju, *CrystEngComm* **2012**, *14*, 2489–2493; b) P. J. Halfpenny, K. J. Roberts, J. N. Sherwood, *J. Mater. Sci.* **1984**, *19*, 1629–1637; c) D. H. C. Wendy, G. C. Weatherly, *J. Mater. Sci. Lett.* **1989**, *8*, 1350–1352; d) X. Liao, T. S. Wiedmann, *J. Pharm. Sci.* **2004**, *93*, 2250–2258; e) L. J. Taylor, D. G. Papadapoulos, P. J. Dunn, A. C. Bentham, J. C. Mitchell, M. J. Snowden, *Powder Technol.* **2004**, *143*, 179–185; f) L. J. Taylor, D. G. Papadapoulos, P. J. Dunn, A. C. Bentham, N. J. Dawson, J. C. Mitchell, M. J. Snowden, *Org. Process Res. Dev.* **2004**, *8*, 674–679.

[11] a) W. C. Duncan-Hewitt, D. L. Mount, A. Yu, *Pharm. Res.* **1994**, *11*, 616–623; b) K. J. Ramos, D. F. Bahr, *J. Mater. Res.* **2007**, *22*, 2037–2045; c) K. J. Ramos, D. E. Hooks, D. F. Bahr, *Philos. Mag.* **2009**, *89*, 2381–2402; d) R. J. Roberts, R. C. Rowe, P. York, *Int. J. Pharm.* **1995**, *125*, 157–162; e) S. Chattoraj, L. Shi, C. C. Sun, *CrystEngComm* **2010**, *12*, 2466–2472.

[12] M. S. R. N. Kiran, S. Varughese, C. M. Reddy, U. Ramamurty, G. R. Desiraju, *Cryst. Growth Des.* **2010**, *10*, 4650–4655.

[13] S. Varughese, M. S. R. N. Kiran, K. A. Solanko, A. D. Bond, U. Ramamurty, G. R. Desiraju, *Chem. Sci.* **2011**, *2*, 2236–2242.

[14] a) M. B. Dines, *J. Chem. Educ.* **1974**, *51*, 221; b) H. Hu, J. C. Martin, M. Xiao, C. S. Southworth, Y. Meng, L. Sun, *J. Phys. Chem. C* **2011**, *115*, 5509–5514; c) F. J. Di Salvo, R. Schwall, T. H. Geballe, F. R. Gamble, J. H. Osiecki, *Phys. Rev. Lett.* **1971**, *27*, 310–313.

[15] a) C. Sun, D. J. W. Grant, *Pharm. Res.* **2001**, *18*, 274–280; b) C. G. Pierpont, *Proc. Indian Acad. Sci.* **2002**, *114*, 247–254; c) R. Bandyopadhyay, D. J. W. Grant, *Pharm. Res.* **2002**, *19*, 491–496; d) C. Sun, D. J. W. Grant, *Pharm. Res.* **2004**, *21*, 382–386; e) Y. Feng, D. J. W. Grant, *Pharm. Res.* **2006**, *23*, 1608–1616; f) C. C. Sun, H. Hou, *Cryst. Growth Des.* **2008**, *8*, 1575–1579.

[16] a) C. M. Reddy, S. Basavoju, G. R. Desiraju, *Chem. Commun.* **2005**, 2439–2441; b) C. M. Reddy, M. T. Kirchner, R. C. Gundakaram, K. A. Padmanabhan, G. R. Desiraju, *Chem. Eur. J.* **2006**, *12*, 2222–2234.

[17] a) C. M. Reddy, R. C. Gundakaram, S. Basavoju, M. T. Kirchner, K. A. Padmanabhan, G. R. Desiraju, *Chem. Commun.* **2005**, 3945–3947; b) C. M. Reddy, K. A. Padmanabhan, G. R. Desiraju, *Cryst. Growth Des.* **2006**, *6*, 2720–2731; c) C. M. Reddy, G. R. Krishna, S. Ghosh, *CrystEngComm* **2010**, *12*, 2296–2314.

[18] J. D. Bauer, E. Haussuhl, B. Winkler, D. Arbeck, *Cryst. Growth Des.* **2010**, *10*, 3132–3140.

[19] R. Foster in *Organic Charge Transfer Complexes*, Academic Press, New York, **1968**, pp. 216–251.

[20] C. K. Prout, T. Morley, I. J. Tickle, J. D. Wright, *J. Chem. Soc. Perkin Trans. 2* **1973**, 523–527.

[21] G. Toussaint, E. Burov, J. P. Avouac, *Tectonics* **2004**, *23*, TC6003.

[22] D. Olusanmi, K. J. Roberts, M. Ghadiri, Y. Ding, *Int. J. Pharm.* **2011**, *411*, 49–63.

[23] J. D. Wright, K. Yakushi, H. Kuroda, *Acta Crystallogr. Sect. B* **1978**, *34*, 1934–1938.

[24] J. C. Tan, A. K. Cheetham, *Chem. Soc. Rev.* **2011**, *40*, 1059–1080.

[25] W. C. Oliver, G. M. Pharr, *J. Mater. Res.* **1992**, *7*, 1564–1583.

[26] a) P. Kumar, M. S. R. N. Kiran, *Nanoscale Res. Lett.* **2010**, *5*, 1085–1092; b) P. Kumar, M. S. R. N. Kiran, *Sci. Technol. Adv. Mater.* **2010**, *11*, 025003–025010.

Received: March 9, 2012
Published online: June 11, 2012

